Soft Matter

PAPER

View Article Online
View Journal | View Issue

Cite this: *Soft Matter*, 2024, **20**, 4935

Significance of *in situ* quantitative membrane property–morphology relation (QmPMR) analysis†

Zachary Nicolella,[a] Yukihiro Okamoto, *[a] Nozomi Morishita Watanabe, [a] Gary Lee Thompson[b] and Hiroshi Umakoshi *[a]

Received 26th February 2024,
Accepted 27th May 2024

DOI: 10.1039/d4sm00253a

rsc.li/soft-matter-journal

Deformation of the cell membrane is well understood from the viewpoint of protein interactions and free energy balance. However, the various dynamic properties of the membrane, such as lipid packing and hydrophobicity, and their relationship with cell membrane deformation are unknown. Therefore, the deformation of 1,2-dipalmitoyl-*sn*-glycero-3-phosphocholine (DPPC) and oleic acid (OA) giant unilamellar vesicles (GUVs) was induced by heating and cooling cycles, and time-lapse analysis was conducted based on the membrane hydrophobicity and physical parameters of "single-parent" and "daughter" vesicles. Fluorescence ratiometric analysis by simultaneous dual-wavelength detection revealed the variation of different hydrophilic GUVs and enabled inferences of the "daughter" vesicle composition and the "parent" membrane's local composition during deformation; the "daughter" vesicle composition of OA was lower than that of the "parents", and lateral movement of OA was the primary contributor to the formation of the "daughter" vesicles. Thus, our findings and the newly developed methodology, named *in situ* quantitative membrane property–morphology relation (QmPMR) analysis, would provide new insights into cell deformation and accelerate research on both deformation and its related events, such as budding and birthing.

Significance

We applied fluorescence ratiometric imaging analysis with a simultaneous two-wavelength detection system to study the deformation of GUVs based on membrane hydrophobicity and morphological parameters. Our methodology can pursue variations in the hydration degree and morphology in the same single GUV during thermal cycles. Thus, our methodology can consider the heterogeneous and dynamic properties of the cell membrane during deformation, which cannot be achieved through mechanical-based studies. This method enables the analysis of the properties and composition of parent vesicles and newborn daughter vesicles without separation. Hence, our methodology (QmPMR) will provide deeper insights into deformation and its related events, such as the budding and birthing of cell membrane-related vesicles.

1. Introduction

Biological cells undergo various processes in which the standard shape of the cell is deformed, such as adhesion, exocytosis and endocytosis, migration/invasion, fusion, budding, division, *etc.*[1] These processes are widely known to be modulated by enzymes and proteins, but more importantly this modulation comes in the form of adjusting the local composition of the plasma membrane, including the local phospholipid, cholesterol, and membrane bound molecules, such as proteins and carbohydrates.[2] This remodeling causes local disturbances in both the energy balance and curvature of the membrane initiating deformation.[3] These processes are omnipresent in the normal cellular life cycle, and understanding the dynamics actions undertaken by the lipid membrane is essential in understanding these cellular deformation processes.

In addition, research pertaining to the origin of life requires the mystery of lipid membrane deformation to be resolved. In the primordial soup of early Earth lakes, replicating protocells were most likely formed *via* simple vesicular structures that underwent simple chemical reactions.[4] However, the development of life requires a stable and reproducible mechanism for cell division and growth. Through a cycle of self-assembly of vesicle-like structures, replication of structures *via* budding or birthing, and growth of newly formed daughter vesicles, a process for the replication of pre-life cells could be established.

[a] *Division of Chemical Engineering, Graduate School of Engineering Science, Osaka University, 1-3 Machikaneyama-cho, Toyonaka, Osaka 560-8531, Japan. E-mail: okamoto.yukihiro.es@osaka-u.ac.jp, umakoshi.hiroshi.es@osaka-u.ac.jp, b-ice@cheng.es.osaka-u.ac.jp*

[b] *Rowan University, Rowan Hall, Room 333 70 Sewell St., Ste. E Glassboro, NJ 08028, USA*

† Electronic supplementary information (ESI) available. See DOI: https://doi.org/10.1039/d4sm00253a

For the replication and deformation of prebiotic cells, multiple mechanisms have been reported through different types of stimuli, such as the addition of small unilamellar vesicle (SUV) to giant unilamellar vesicle (GUV) suspensions, changes in pH, chemical reactions within the vesicle, or temperature changes,[5–9] which can imitate the environment of the prebiotic Earth. As a result, uncovering the mechanism and behavior of deformation cannot only reveal more important information about these events but can also help illuminate the mystery of the origins of life.[10]

Owing to its significant importance, the deformation phenomenon has been extensively studied. Many studies have reported deformation *via* physical–chemical theory (free energy), simulation, and analysis of physical membrane properties, such as membrane tension, bending modulus, and size parameters. These studies have well described the theory between deformation and its following phenomena. However, these mechanical based studies lack information about the vesicle deformation in real time, and rely on post-deformation analysis based on force modeling and computer simulation; (i) cell membranes show heterogeneous properties by clustering raft nanodomains and deformation. This issue manifests in relation to the biological plasma membrane that shows highly heterogenous structures in the form of nanodomains and lipid rafts.[11] However, this heterogeneity was not considered in previous studies. (ii) In some cases, after morphological changes, budding or birth of vesicles are observed and are studied in terms of mechanical properties and free energy change.[12] However, these studies have not reported the membrane properties and composition of newborn vesicles because of the difficulty of analysis. (iii) Studies using a similar analysis method to the one presented here are often performed in the steady state (at a constant temperature) and are sometimes difficult to conduct in a time-lapse manner in a non-equilibrium state, such as heat flow, which imitates the environment of the cell and primordial protocells. Therefore, a study of deformation is required to overcome these problems and meet these demands.

Due to the high focus on the mechanical membrane properties and free energy of deformation, the influence of interfacial membrane properties such as hydrophobicity is widely unaccounted for. These interfacial properties are widely determined by the interaction between the solvent (generally water) and the lipid bilayer, where the fluorophores in various probes are relaxed differently based on the surrounding solvent environment.[13] These interfacial properties manifest changes in the lipid membrane in many ways, the most popular of which is the classification of ordered and disordered phases of the membrane.[14] Additionally, its influence can be seen in cancer progression, as higher membrane fluidity in tumor cells enhances cell migration, accompanied by deformation and formation of blebs.[15,16] The influence of these interfacial membrane properties and deformation of the lipid membrane is intrinsically connected and should be explored further.

Thus, the focus of this research was developing a method to perform real time quantification of membrane deformation in the form of vesicles' interior budding and birthing *via* pores. This quantification was classified as hydrophobicity of the interfacial region and packing from the analysis of lipid membrane fluorescent probes. Such properties are essential in understanding the interior budding and birthing process of GUVs as a result of the potential to qualify the membrane during the aforementioned phenomena. Properties derived from the fluorescent probes not only are very easy to measure and quantify but, they are also intrinsically connected to the biophysical properties like bending rigidity, membrane tension, and NMR order parameters.[17–19] Such biophysical properties are typically difficult to measure requiring specific apparatus or being limited by a certain range of compositions. Hence using properties collected *via* the analysis of fluorescent probes simplifies the analysis of the deformation phenomena while also making it much more approachable due to the ease of collecting fluorescence data.

The selection of the components of the GUVs is probably the most important parameter when conducting any lipid-based research. In this study DPPC and OA were selected as the components of the model GUVs. Above 30 mol% OA in the GUVs, the yield and size distribution of vesicles became undesirably low; hence, the upper limit of this study regarding the OA composition was 30 mol%. While this limit does make it difficult to establish a trend based on the OA concentration, this range still does allow for the expansion and explanation of the analysis method presented here. Phosphatidylcholine is the major lipid constituent of eukaryotic cell membranes,[20] and DPPC has consistently been used before in studies relating to deformation phenomena, specifically relating to the research conducted by the Imai group.[5,21,22] Fatty acids, specifically OA, have also been shown to undergo deformation in various other systems.[6,23] Additionally fatty acids have been increasing in prominence as a research topic due to their recently uncovered connection to developmental health based on fatty acid profile consumption.[24] Another important parameter of the selection of these two molecules was the mixing of a neutral curvature and negative curvature lipid, this type of mixture has been shown to be able to produce thermally induced internal budding deformation.[22] Finally, since the transition temperature of DPPC (41 °C) is rather close to room temperature, the cycling of temperature from 22.5 to 48 °C is simplified due to the lack of condensation, freezing, or evaporation around the test chamber. The combination of the two components previously shown to be able to undergo deformation, the combination of a neutral and negative curvature, and the proximity to room temperature of the transition temperature made DPPC and OA a viable choice for investigation into the membrane properties of the lipid membrane while undergoing deformation.

Furthermore, we aimed to analyze the properties and composition of the newborn and original parents' vesicles during deformation. For this purpose, we adopted a dual-wavelength detection system[25] with a solvatochromic dye (LipiORDER) for time-lapse and single GUV analysis and successfully obtained information about the membrane hydrophobicity in a parent GUV and in newborn vesicles. By using information about the compositional changes in the parent and newborn daughter vesicles, inferences can be made regarding the local heterogeneity of the membrane. Compared to previous research on

deformation in lipid membranes,[3,5–8] our method allows for direct observation of membrane properties during deformation. By coupling membrane property evaluation with deformation in real time, we named this methodology *in situ* quantitative membrane property–morphology relation (QmPMR) analysis, and deep insights and relationships can be established connecting the activity and behavior of the membrane during deformation. The benefits of this deformation analysis technique are mainly exemplified by the concurrent analysis of lipid packing during deformation of the membrane and the ability to check the packing of newly formed daughter vesicles *via* the induced deformation. In addition, using this analysis we can also make some inferences about the membrane behavior during deformation, such as the lateral mobility of OA creating a difference in membrane curvature during the thermal cycle most likely being the driving force of deformation within the membrane or the relative composition of the daughter and parent vesicles.

2. Experimental section

2.1 Materials

Dipalmitoylphosphatidylcholine (DPPC, T_m = 41 °C), 1,2-dioleoyl-*sn-glycero*-3-phosphocholine (DOPC, T_m = −17 °C), and 1,2-dipalmitoyl-*sn-glycero*-3-phosphoethanolamine-*N*-(lissamine rhodamine B sulfonyl) (DPPE-RHO) were purchased from Avanti Polar Lipids, Inc. (Alabaster, AL, USA). Oleic acid (99% purity) (OA) and sucrose were purchased from Sigma-Aldrich Co. LLC (St. Louis, MO, USA). LipiORDER was purchased from Funakoshi Co., Ltd (Tokyo, Japan), and a stock solution (3.0 mM) was prepared in dimethyl sulfoxide (Kanto Chemical Co., Inc., Tokyo, Japan). Chloroform, methanol, ethanol and 6-dodecanoyl-*N*,*N*-dimethyl-2-naphthylamine (Laurdan) were obtained from Wako Pure Chemical Industries Ltd (Osaka, Japan). A Laurdan stock solution was prepared using ethanol at a concentration of 10 mM. Lipids were further processed into a 10 mM stock solution; DPPC was dissolved in 100% chloroform, while OA was diluted in an 80% chloroform/20% methanol solution. All reagents were used as received without further purification. Ultrapure water was prepared using Direct-Q® UV3 (Merck Millipore Co., Tokyo, Japan). A sucrose solution (200 mM) was prepared using ultrapure water. Chemical structures of all lipids and probes used can be found in Fig. 1.

2.2 Preparation of giant unilamellar vesicles (GUVs)

GUVs in this study were prepared using the electroformation method (more information is provided in the ESI†).[26,27] The stock lipid solution was further diluted into a 90% chloroform/10% methanol solution to be 2.5 mM at the targeted

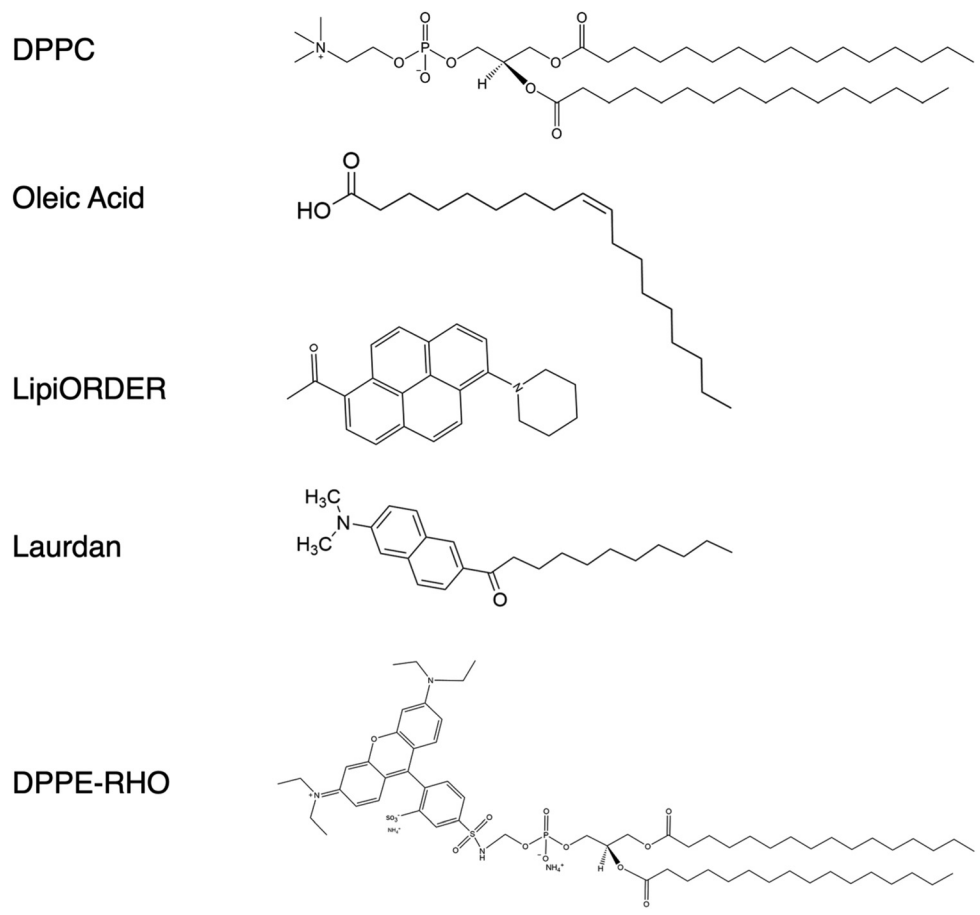

Fig. 1 Chemical structure of all lipids and probes used in this research.

composition. The composition of the GUVs ranged from 70 mol% DPPC/30 mol% OA to 100 mol% DPPC. The lipid solution (2.5 mM, 2.5 mL) was then deposited on two indium tin oxide (ITO)-coated glasses (30–60 Ω sq^{-1}, Sigma–Aldrich Co. LLC, St. Louis, MO, USA) and placed directly onto a spin coater (Opticoat MS-A100, Mikasa, Tokyo, Japan) at 600 RPM for 4 min. The resulting lipid film on the ITO glass was then transferred to a high-vacuum desiccator for a minimum of 2 h to remove all solvent traces. After desiccation, the coated ITO glass was clamped together by sandwiching a 0.5 mm silicon spacer, and then approximately 1.5 mL of 200 mM sucrose solution was added to the silicon spacer, this chamber was sealed, and the pH of this solution is approximately 6.5; its effects on the protonation of OA will be discussed later in the manuscript. This chamber was then connected to a function generator (SG-4262, Iwatsu, Tokyo, Japan) and heated to approximately 50 °C to facilitate the formation of uniform vesicles.[28] The sinusoidal waveform of the function generator was run at 10 Hz and 10 Vpp for 90 min, and then at 100 Hz and 10 Vpp for an additional 30 min. The completed GUVs were removed from the chamber and stored at room temperature. GUVs were typically used within 12 h after preparation and were disposed of 48 h after preparation.

Fluorescent dyes DPPE-RHO, LipiORDER, and Laurdan were used for the imaging of single GUV and for membrane hydrophobicity and membrane packing analysis in both single GUVs and bulk GUV suspensions. In the case of DPPE-RHO, this dye was added to the 2.5 mM lipid solution at a concentration of 0.5 mol% before spin coating. LipiORDER and Laurdan were added immediately after electroformation at dye-to-lipid molar ratios of 1/250 and 1/100, respectively.[29,30] Immediately after adding the LipiORDER or Laurdan solution to the GUV suspension, it was placed in a heater (CTU MINI, TAITEC, Saitama, Japan) for 2 h at 50 °C, after which the temperature was reduced to approximately 25 °C or room temperature for over 2 h.

2.3 Imaging and analysis of single GUV under heating and cooling

The chamber for GUV observation was fabricated by creating a 5 mm diameter hole in a 0.5 mm thick section of silicon,

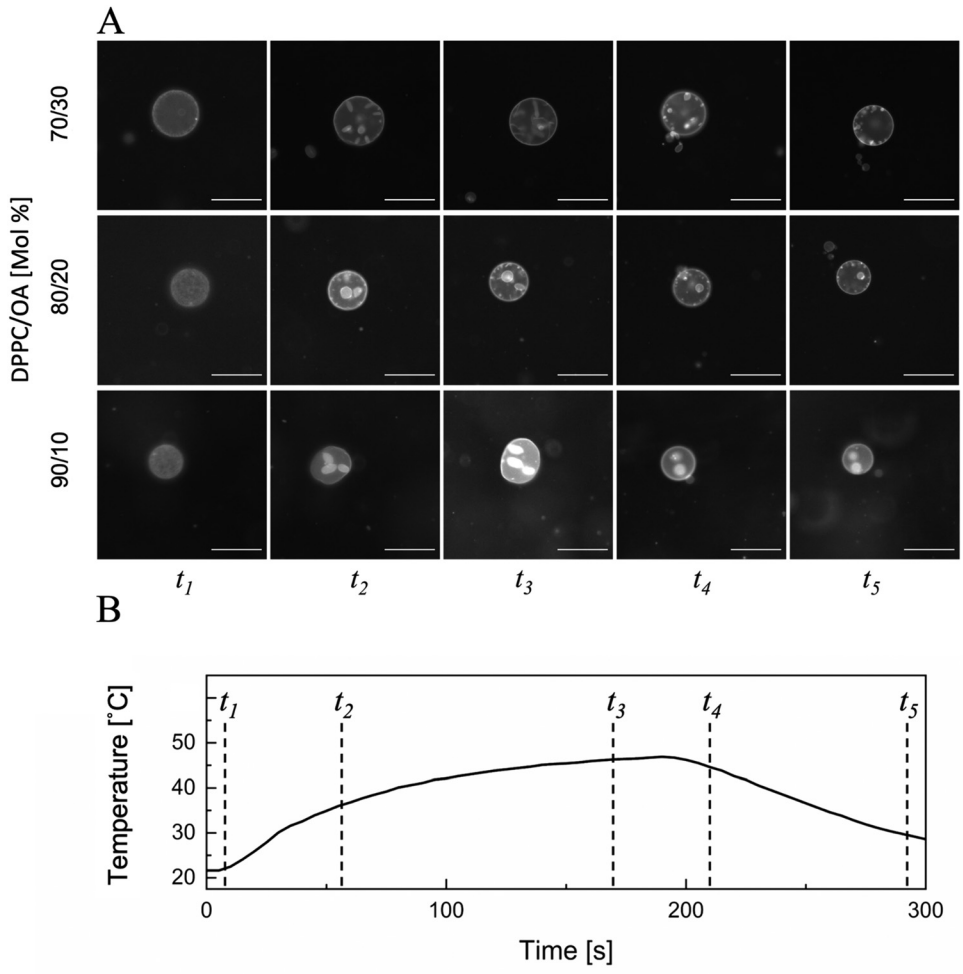

Fig. 2 Representative time-lapse epi-fluorescence images of GUVs (A) with different composition at different temperatures (t_1–t_5) during the temperature cycle shown in (B). Each image set is a representative set of approximately 25 samples per composition (scale bar = 50 μm). Each set of images display one representative sample of the respective composition. Conditions: dye, DPPE-RHO; others, as described in the Experimental section.

pressing it into a glass side, and sealing it with a cover slip. A temperature-controlled thermoplate (Tokai Hit, Fujinomiya, Japan) was used to precisely control the temperature of the samples. In the case of epifluorescence imaging with an upright fluorescence microscope, the observation chamber was placed above the temperature-controlled plate, whereas in confocal imaging with an inverted fluorescence microscope, the temperature-controlled plate was placed on top of the observation chamber and held in place using a weight. All experiments followed a strict heating and cooling protocol of 3 min of heating to 48 °C, followed by 2 min of cooling; this temperature profile is shown in Fig. 2(B). This thermal cycle was repeated for 95 individual GUV samples from approximately 40 different populations of the GUV suspension.

Fluorescence imaging was conducted using DPPE-RHO and LipiORDER dyes. All images were taken using a fluorescence microscope (BX53, Olympus, Tokyo, Japan) with a 20× lens (NA 0.50) (UplanFLN, Olympus, Tokyo, Japan) and captured using a complementary metal oxide semiconductor (CMOS) camera (ORCA-Fusion, HAMAMATSU Photonics, Japan). Excitation light for imaging was generated using a mercury lamp (130 W, U-HGLGPS, Olympus, Tokyo, Japan). The filter sets for each fluorescent dye were as follows: for DPPE-RHO, excitation filters: 530–50 nm, dichroic mirror: 570 nm, and barrier filter: ∼575 nm; for LipiORDER, excitation filters: 389/38 nm, dichroic mirror: 414 nm, and barrier filter: ∼450 nm. In the case of LipiORDER for dual-wavelength imaging, image-splitting optics (W-VIEW GEMINI A12801-01, HAMAMATSU Photonics, Japan) containing filter sets (dichroic mirror: 560 nm and barrier filters: ∼510/84 nm and ∼574 nm) was connected to a fluorescence microscope and CMOS camera. Images and videos were recorded with a 200 ms exposure time, and a low laser power was used to suppress photobleaching. All image processing was conducted in the cellSens Dimension (CS-DI5-SET, Olympus, Tokyo, Japan). After removing the background fluorescence, which is defined as the portion of the image that did not contain vesicles, the membrane packing of the GUV membrane was estimated using the fluorescence intensity ratio as follows:

$$\text{Membrane packing} = (I_{574}/I_{510}) \quad (1)$$

where F_{574} and F_{510} are the fluorescence intensities through the 574 nm and 510/84 nm filters, respectively. The measured portion of the image only contains the target vesicle and is an average value of the complete membrane packing, thus allowing the separation of target vesicles and the background of the image or other vesicles. This grants us the ability to measure the packing of singular vesicles. This value represents the packing of the membrane since the emission of LipiORDER changes based on the ordering of the membrane where the ''liquid ordered'' or ''gel'' phase and ''liquid disordered'' phase emit at 510 nm and 574 nm respectively. This is due to the solvatochromatic properties of the pyrene-based probe, representing a change in polarity due to the lipophilicity of the environment surrounding the LipiORDER probe. However, for the sake of simplicity it will be referred to as membrane packing in the rest of this work due to the interchangeable use of the terms membrane order and membrane packing.

All confocal imaging was performed using an Olympus IX83 microscope (Olympus, Tokyo, Japan) with a 20× lens (NA 0.80) (UplanXApo, Olympus, Tokyo, Japan) powered by a MAICO confocal unit (HAMAMATSU Photonics, Japan). GUVs stained with DPPE-RHO were used for all confocal imaging experiments. The images of GUVs were obtained with a 561 nm laser and all optical image processing was performed using HCImage (HAMAMATSU Photonics, Hamamatsu, Japan). To prevent the photodeformation of GUVs, a low laser power of less than 5 mW was used.[31]

2.4 Hydrophobicity degree analysis in bulk GUV suspension

The mean values of the GUV membrane hydrophobicity under a pseudo-equilibrium state were estimated using Laurdan containing GUV suspension, in which the total concentrations of lipids and Laurdan were 100 and 1 μM, respectively. All measurements were performed using an FP-8500 spectrofluorometer (JASCO Corporation, Tokyo, Japan). The emission spectra were recorded at an excitation wavelength of 340 nm. The general polarization (GP_{340}), the membrane hydrophobicity, was calculated as follows,

$$GP_{340} = (I_{440} - I_{490})/(I_{440} + I_{490}) \quad (2)$$

where I_{440} and I_{490} represent the fluorescence intensities of Laurdan at 440 and 490 nm, respectively. This value is classified as hydrophobicity since the emission spectrum of the solvatochromic probe Laurdan is mainly determined by the surrounded water molecules present between the phosphate groups within the hydrophilic portion of the lipid bilayer.[32] This value can range from 1 to −1 with 1 representing the most possible hydrophobic environment, meaning the absence of water. The sample temperature was adjusted at a rate of 5 °C, with a time interval of 5 min between each temperature change. Each sample was measured three times for each temperature and was used for one temperature cycle and disposed of immediately afterward.

3. Results and discussion

3.1 Deformation of DPPC/OA GUVs *via* heating cycles

A binary mixture of GUV made from 70/30 mol% to 100/0 mol% (DPPC/OA) was deformed *via* a heating and cooling cycle from 22.5 °C to 48 °C. This range of temperatures was selected because 22.5 °C is relatively close to room temperature and 48 °C is well above the transition temperature (T_m) of all compositions tested.[33] By heating and cooling GUVs for over 5 min in the form of a 3-minute heating period followed by a 2-minute cooling period, the overall pattern of deformation, formation, and birthing of a daughter vesicle was observed, as shown in Fig. 2(A). In general, the deformation patterns induced in vesicles containing OA were very similar. A more detailed view of the deformation in OA-containing vesicles can be found in the ESI,† Movies S1–S3, representing 70/30, 80/20, and 90/10 (DPPC/OA mol%), respectively. Upon applying heat

to the vesicles, GUVs quickly deform into a stomatocyte shape, represented by the formation of daughter vesicles within the membrane. This deformation pattern was observed in all the vesicles containing OA. In all the OA-containing vesicles tested, approximately 1–10 daughter vesicles (approximately 1–20 μm in size) were formed in a single-parent GUV. In parent GUVs with higher percentages of OA, the daughter vesicles tended to be more tubular (ESI,† Movie S1). This was most likely due to the higher percentage of OA within the daughter vesicles compared to the daughter vesicles from GUVs containing a higher ratio of DPPC. The images found in Fig. 2 show small bright spots that could possibly be interpreted as small lipid aggregates, however observation of the vesicles undergoing the thermal cycle show these small bright spots are fluid and moving throughout the GUV indicating that they are in fact unilamelar vesicles around 1 μm in size. Upon increasing the zoom during observation it was also seen that these bright spot look like standard vesicles as well.

After the formation of daughter vesicles, GUVs underwent a period of rapid expansion due to the initiation of phase transition. After this period of expansion, the sample reached its peak temperature at 48 °C after 3 min of heating, and a 2-minute cooling period then commenced. Upon the introduction of the cooling period, the membrane experienced rapid shrinking of its total area. This shrinkage is due to the transition temperature of the membrane,[34] which causes the membrane to change into a more ordered state. During this period of membrane shrinkage, the tension of the membrane was greatly increased owing to the very rapid decrease in surface area, and thus, a pore was opened to alleviate this increase in tension.[35] This opening allows the previously formed interior daughter vesicles to exit from the parent vesicles *via* expulsion. Multiple daughter vesicles can be expelled simultaneously depending on the size of the daughter vesicle(s) and the distance between the daughter vesicle(s) and the recently opened pore. This phenomenon occurred in approximately 50% of the parent vesicles (n = 95). After expulsion of the daughter vesicles, the pores remained open for a total of a few seconds and then quickly closed. The parent vesicle then returned to its original circular shape, as reflected upon the first observation of the vesicle. A second heating cycle was conducted to determine whether this phenomenon was repeatable and if it induced the birth of granddaughter vesicles or a second daughter from the original parent. Generally, during the second heating cycle, the original parent vesicles underwent a significantly different deformation pattern than that observed during the first heating cycle. This is best exemplified in the ESI,† by Movies S1–S3 representing 70/30, 80/20, and 90/10 DPPC/OA mol% systems, respectively, where the deformation was much more random in nature and the vesicles underwent a change into a much more noncircular shape. This non-specific shape can be exemplified as extremely oblate shapes showing very elongated ovals. In general this deformation follows a similar cycle as found in research in the Imai group, where vesicles with an 8 : 2 molar ratio of DPPC/DLPE were put under a temperature cycle to perform an exterior budding process.[22] Thus, this non-specific shape is most likely due to a change in the parent vesicle composition in comparison to the first heating cycle. The long oblate shapes are very similar to those presented in that research, and this is most likely due to the higher percentage of inverse cone shaped lipids in the membrane after the first heating cycle since the majority of OA is transferred to the daughter vesicle during the budding birthing process (discussed later in detail). Due to the formation and separation of daughter vesicles, the lipid composition ratio in the parent vesicles changed, and all OA-containing vesicles exhibited similar behavior. Finally, there was no second birth of a granddaughter (a vesicle born from a previously birthed daughter vesicle) or an additional daughter vesicle during the second heating cycle.

The deformation pattern in wholly DPPC vesicles was quite different from that in OA-containing GUVs. Multiple examples of the deformation of 100/0 (DPPC/OA) GUVs are shown in ESI,† Fig. S2. The deformation of DPPC only GUVs resulted in a large display of different pathways of deformations. These deformation pathways include the budding and birthing pathway found in the OA containing GUVs, mild shape deformation, elongation into a large oblate shape, and outward budding deformation. This is similar to other reports on the deformation of pure DPPC vesicles where multiple types of deformations were observed, from stomatocyte formation[36] to minimal deformation and domain formation.[37] Observation of these multiple pathways of deformation didn't reveal any overarching pattern of why certain GUVs undergo certain deformation pathways and seems to be random. A single sample of GUVs include all deformation patterns shown in the ESI,† Fig. S2 and these patterns also hold true across different GUV populations.

Therefore, *via* the observations made from the deformation phenomena, it can be seen that the inclusion of OA leads to a reduction in the number of deformation pathways, resulting in only the interior budding pathway being present. This is most likely concerning the position and bending of DPPC and OA in this system. Firstly, cone-shaped lipids, in this case OA due to its small head group and double bond, are more likely to be sorted into the inner leaflet of the membrane, due to the natural negative curvature of this cone shaped lipid.[21,38] Furthermore, the curvature of DPPC and OA mixed membranes is also less than zero and with increasing amounts of OA it becomes increasingly negative. As explained later, the nanodomain formation of highly concentrated OA regions in the inner leaflet leads to regions of high negative curvature most likely leading to the interior budding phenomena.[39]

3.2 Size dependence of GUV birthing

Previous research based on simulations by the Imai group[12] showed a similar phenomenon with DPPC/DPPE vesicles as ours and established a relationship between the ratio ($\text{Ratio}_r = r_d/r_p$) of the radius of the daughter vesicle (r_d) and the parent vesicle (r_p). In our study, we found a relationship between the success of the birthing process and the size of parent vesicles in all OA-containing vesicles. Fig. 3 shows histograms of the daughter and parent vesicle radii (Fig. 3-i and ii) and their ratios (Fig. 3-iii and iv) for successful and failed birthing. This

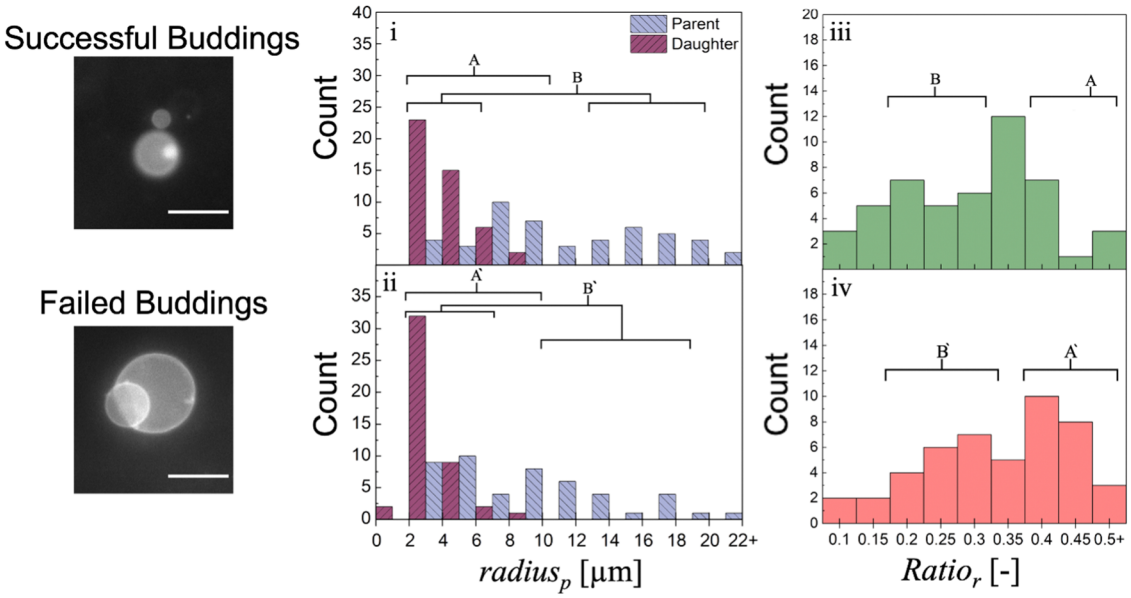

Fig. 3 Size distributions of the parent and daughter GUVs in (i) successful and (ii) failed birthing cases. Size ratio distribution in (iii) successful and (iv) failed birthing cases. Conditions: dye, DPPE-RHO; others, as described in the Experimental section (scale bar = 40 μm).

data accounts for all OA containing GUVs tested, as the behavior between them was similar, the radii of the vesicles was measured at approximately a temperature of 25 °C. A failed birthing was defined as the absence of separation between the parent and daughter vesicles over a short period of time, approximately one minute, whereas a successful birthing showed clear and visible separation, as shown in Fig. 3. Of the 95 vesicles tested, 48 completed a successful birthing process, whereas 47 did not. An equal number of failures and successes allowed for a more equivalent comparison between the two groups. There is a visible trend that the larger the parent vesicles, the more likely they are to succeed in birthing. This can also be explained by the average radius of the successful and failed groups, wherein the average radii were 13.2 and 10.6 μm for the successfully birthed and failed-birthed groups, respectively. Compared with smaller vesicles, larger vesicles have a greater change in area from the peak of the temperature cycle to the end of the cooling period. This larger area change thus leads to an increased change in membrane tension during the same period; hence, a larger GUV has a higher likelihood of opening a pore capable of ejecting a vesicle.[40] This can explain the trend of larger vesicles experiencing a higher rate of successful births.

The daughter vesicle radii distribution in the failed birthing case is much more skewed towards lower radii, with over 85% being below a 6 μm radius. In contrast, the successful regime had a wider distribution of daughter vesicle sizes. Examining the daughter vesicle radii leads to a discussion concerning the ratio of the daughter and parent radii, as shown in Fig. 3-iii and iv. The successful regime can be divided into two groups A and B, and the failed regime can also be divided into two groups A′ and B′. A and A′ represent instances in which the ratio of the daughter and parent vesicle sizes is above 0.40. Looking at these two groups, it is evident that a larger ratio of parent and daughter vesicle sizes is much more likely to cause failure in birth. The same can be applied to the B and B′ groups, showing that larger ratios are more likely to fail and that a much greater rate of success occurs below a ratio of 0.30.

Despite these differences in the behavior, the averages of the ratios in the failures and successes are 0.37 and 0.36, respectively, due to the majority of the successes occurring in the ratio range of 0.35–0.4 contributing to the higher value of the average radius. In previous wet research by the Sakuma group using DPPC/DPPE vesicles, an average radius ratio value average of 0.4 was presented,[7] which is similar to the results obtained here. Regardless of the lipid composition, birthing processes maintain an average optimal ratio of radii (approximately 0.35–0.4). However, other factors determine the success of vesicle birthing, such as the position of the daughter vesicle within the parent or the lifetime of the pore.

3.3 Effect of membrane polarity on birthing

There are multiple membrane properties that help quantify a specific characteristic of the membrane and these are interconnected in various different ways.[17] As mentioned previously this research focuses on the effects of hydrophobicity, measured by Laurdan, and membrane packing, measured by LipiORDER. Hydrophobicity reflects the presence of water within the membrane represented by the polarity of the membrane, and has the ability to influence deformation by varying water the presence leading to a changing area occupied by an individual lipid.[41] There were large differences in the hydrophobicity at the lower and higher ends of the temperature spectrum and slight differences between the different compositions. The mean membrane hydrophobicity in the acyl region was evaluated using the generalized polarization (GP_{340}) value of Laurdan. The

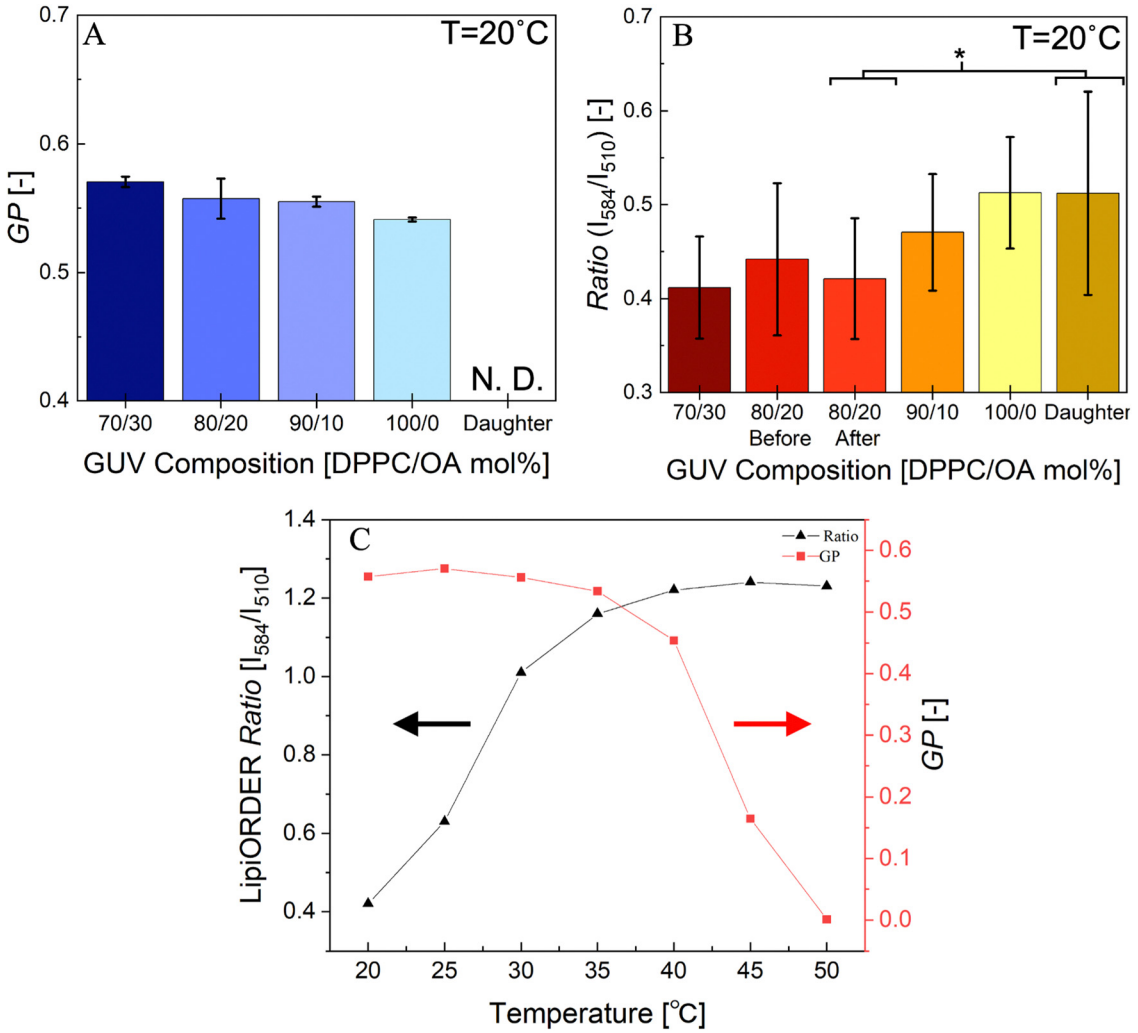

Fig. 4 Analysis of membrane packing and hydrophobicity in (A) GUV suspensions with Laurdan and in (B) a single GUV with LipiORDER of different compositions (DPPC/OA) at 20 °C, 80/20 before and after representing before and after the deformation, and daughter representing the daughter vesicle from 80/20 vesicle, respectively. (C) Temperature dependence of the LipiORDER ratio and GP_{340} values in the 80/20 (DPPC/OA mol%) GUVs. Daughter vesicles were born from 80/20 (DPPC/OA mol%) vesicles (* indicates a p-value of less than 0.05 *via* t-test) (n = 15–35).

increase in temperature caused a transition from the gel phase to the liquid phase in all the compositions tested. Upon cooling, all the tested compositions returned to slightly more hydrophobic and therefore less fluid membrane states (Fig. S3, ESI†). As shown in Fig. 4(A), OA contributes to a higher ordering of the DPPC membrane and thus decreases the hydrophobicity of the membrane, which is similar to previously published research.[42] The decrease in hydrophobicity induced by the addition of OA was largely insignificant, and this trend was maintained throughout the temperature range of 20–50 °C (Fig. S3, ESI†). Contrary to the results of the deformation experiments, one would intuitively assume that the increase in membrane hydrophobicity observed in the OA-containing vesicles would harmoniously reflect a decrease in the magnitude of deformation. However, the increment of OA simultaneously induces other changes in the membrane, such as spontaneous curvature, bending modulus, and other physical variables of the membrane, which cause changes in the deformation pattern, regardless of the hydrophobicity of the membrane.[39]

Laurdan can be used to evaluate the hydrophobicity of a membrane in a GUV suspension. However, due to rapid fluorescence quenching, it is difficult to analyze a single GUV with Laurdan during heating and cooling deformation cycles.[43] Therefore, in this study, the GP_{340} values of Laurdan were used to evaluate the mean values of GUV membrane hydrophobicity under a pseudo-equilibrium state. In contrast, the solvatochromic LipiORDER probe allows for the observation and analysis of a singular GUV over the full period of the heating and cooling cycle *via* fluorescence microscopy. When LipiORDER was excited at 405 nm, its emission was red-shifted based on membrane packing. The different emissions are also linked to the different phases of the lipid membrane: emission at 510 nm represents the L_o phase and emission at 574 nm represents the L_d phase.[29] The resulting fluorescence intensity ratio (I_{574}/I_{510}) indicates the degree of membrane packing, and an increase in the ratio corresponds to an decrease in membrane hydrophobicity.

Fig. 4(B) shows the fluorescence ratio of LipiORDER in each GUV at 20 °C. At first glance, this resulted in the same trend as the analysis with Laurdan. That is, the increasing percentage of OA composition led to an increase in the packing of the membrane and, hence, a decrease in fluidity. LipiORDER's ability to calculate the ratio of a singular vesicle allows for the measurement of birthed daughter vesicles during the heating–cooling cycle. Daughter vesicles formed from 80/20 (DPPC/OA mol%) GUVs were analyzed after departure from their parent counterparts (n = 35). The measured ratio of these daughter vesicles was higher than that of the parent vesicles from which they were born and was much closer to that of pure DPPC vesicles (Fig. 4(B)). Furthermore, the ratio values of 80/20 (DPPC/OA mol%) GUVs were analyzed pre and post deformation, displaying the post deformation values of ratio for 80/20 GUVs are closely in sync with the values for 70/30 GUVs. Further reinforcing the lack of OA in the daughter vesicles since the parent vesicle post deformation becomes slightly more rigid,

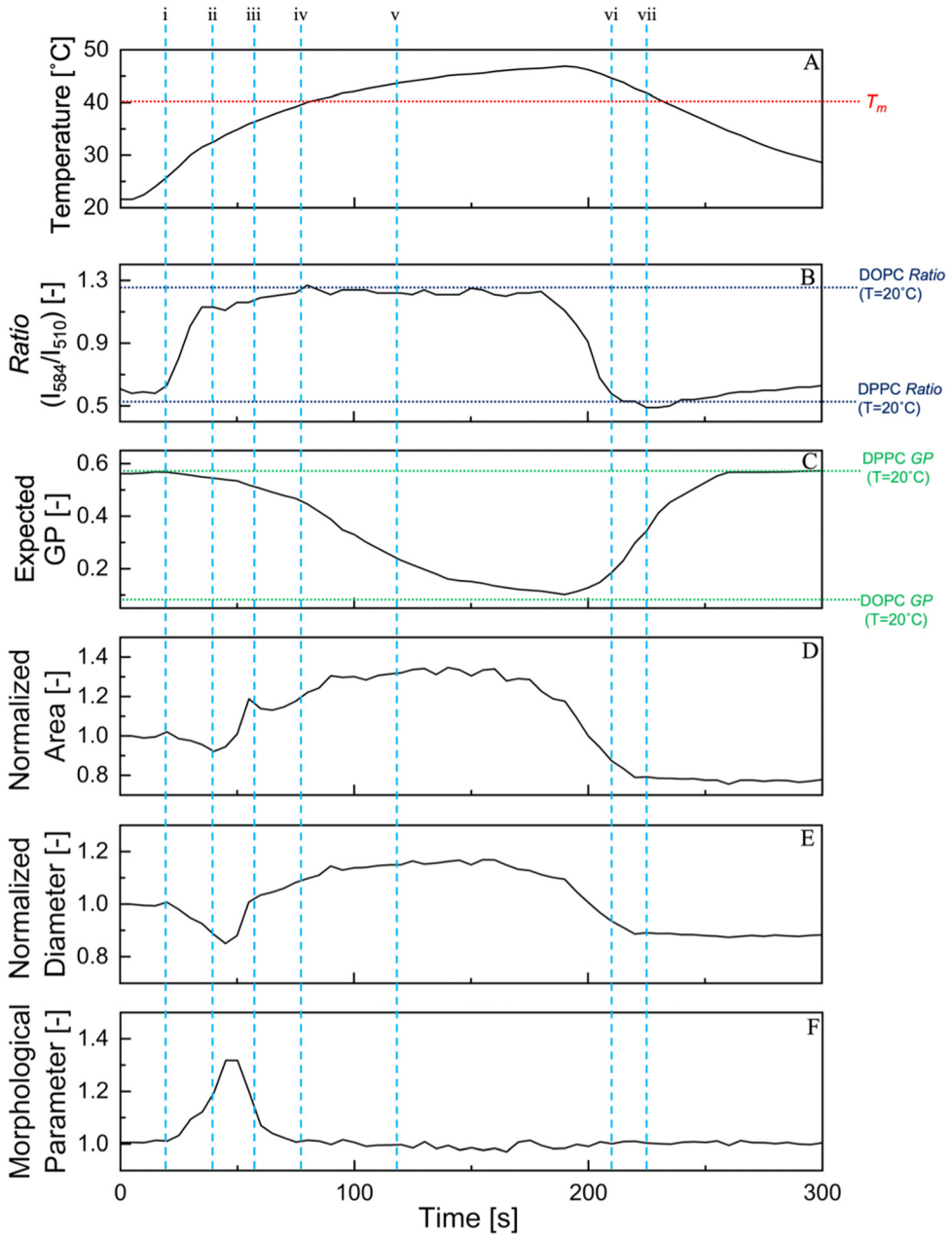

Fig. 5 Variation of membrane hydrophobicity and packing and structures of an 80/20 (DPPC/OA mol%) under (A) the temperature cycle, (B) fluorescence ratio of LipiORDER, (C) expected GP_{340} values, normalized (D) area, (E) diameter, and (F) morphological parameter. Normalized values were normalized to the values at t = 0 (D), (E), and a morphological parameter was calculated with the values of (C) and (D). The vertical lines (i)–(vii) show the points in the deformation cycle, which correspond to the representative confocal images and regions presented in Fig. 6. The number of tested GUVs were 3 and the data is the mean values. The values of DOPC ratio and GP_{340} are provided for ease of the reader to understand the range of ratio and GP_{340} for different lipid suspensions.

indicating a higher amount of OA in the parent vesicle. In addition, Fig. S4 (ESI†) shows that the ratio values did not show size dependency under this condition. These results indicated that the percentage of OA in the daughter vesicles was much lower than that in the parent vesicles.

Fig. 4(C) compares the response of Laurdan and LipiORDER under the influence of the increasing temperature. As expanded upon in the Discussion section there is a difference in the response to the temperature change between these two probes even considering they both respond to the changing of water presence in the lipid membrane. As shown in Fig. 4(C), in general LipiORDER exhibits a change in its emission before the transition temperature while Laurdan shows a large change after the transition temperature.

3.4 Effect of membrane properties on birthing and pore formation

Previous research has widely documented the biophysical response of membranes to rapid temperature changes, which leads to deformation and birthing *via* an opening pore.[44]

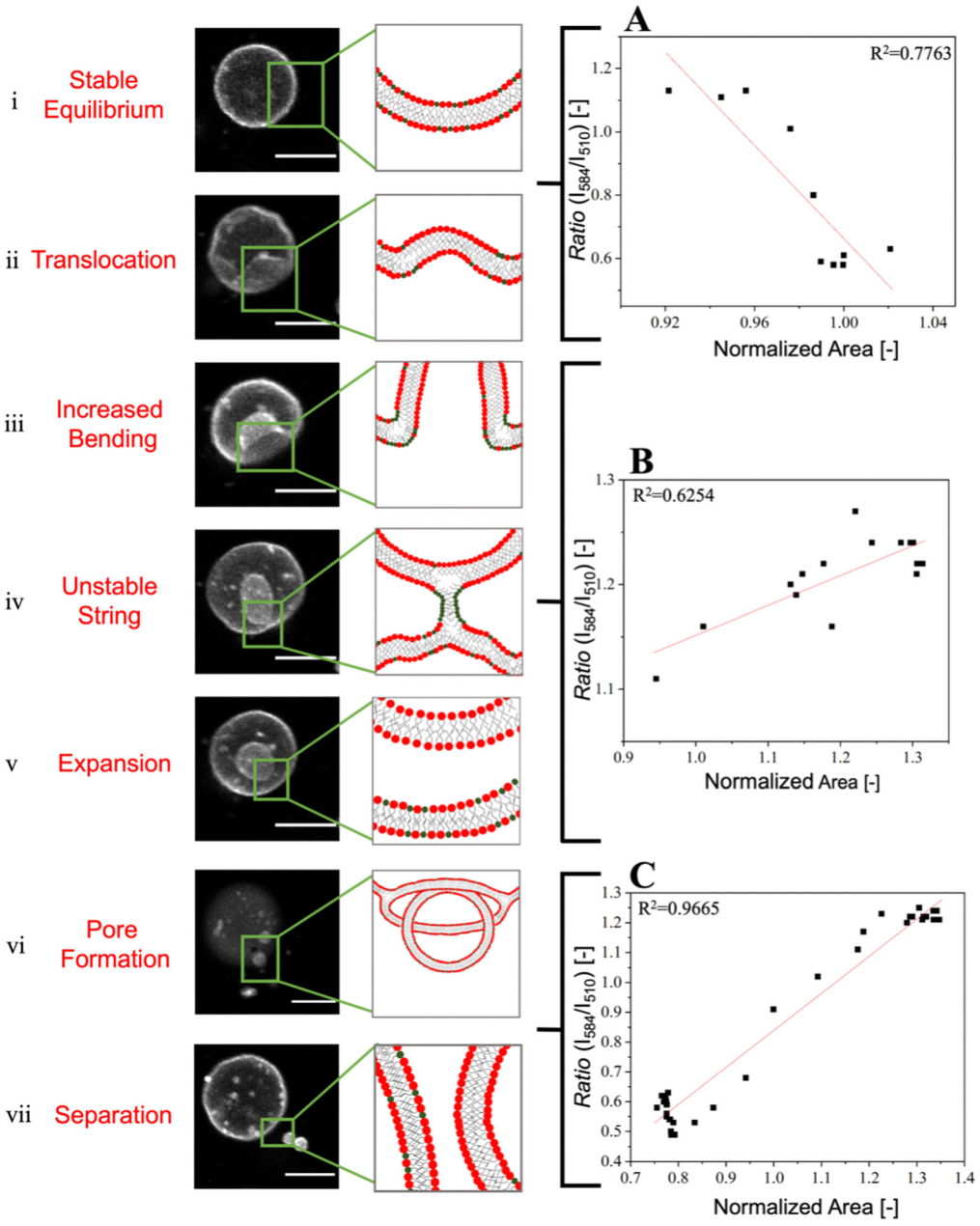

Fig. 6 Confocal images and cartoons of pivotal points in a GUV during heating and cooling cycles. The number corresponds to that in Fig. 5. Conditions: dye, DPPE-RHO; others, as described in the Experimental section (scale bar = 25 μm). A–C describe the relationship between LipiORDER ratio and normalized area during the neighboring time period. The normalized area is from the epi-fluorescence images. The red arrow indicates the formation of a pore (the full video is shown in Movie S7, ESI†).

However, few studies have focused on membrane properties such as hydrophobicity/fluidity in the lipid bilayer and their relationship with physical phenomena. In Fig. 5, the simple structural parameters of a typical 80/20 (DPPC/OA mol%) vesicle undergoing deformation are displayed along with the fluorescence ratio value of LipiORDER and the Laurdan expected GP_{340} values, these values are only for the parent vesicles during deformation and are the average of 3 samples. Within Fig. 5 vertical lines (i–vii) represent important landmark moments within the deformation cycle and are further expanded upon in Fig. 6. The expected GP_{340} value was based on the data in Fig. 4(C) and was used as the expected hydrophobicity index for pseudo-equilibrium states. LipiORDER was measured in step with deformation and recorded as deformation occurred. The structural parameters presented here are the area and diameter of the vesicles, normalized to the value before the temperature cycle begins.

The morphological values (in the case of a spherical shape = 1) are defined as follows:

$$\text{Morphological value} = \frac{A_M}{\pi r^2} \quad (3)$$

where A_M is the measured value of the area and r is the radius of the observed vesicle. The radius of the vesicle was the average of multiple measurements because of the vesicles' noncircular shape. Due to the varied starting areas of the GUVs the areas and diameter were normalized to the starting value of each unique vesicle ($N = 3$) at $t = 0$. The area is a direct measurement of the two dimensional cross section of the vesicle measured in Olympus Cell Sense (Japan).

During the temperature cycle, an increase in temperature from 22.5 °C to 48 °C occurred for 180 s, and the rate of this temperature increase was not constant and slowed towards the peak temperature of 48 °C. The initial deformation was represented by a large change in the morphological value, with a large sudden increase in the fluorescence ratio values of LipiORDER, as shown in Fig. 5-i and ii. This ratio increase occurred over a temperature range of 25–30 °C, which was much lower than the transition temperature of approximately 40 °C. This temperature increase did not accompany a drastic change in the expected GP_{340} value. There are a multitude of reasons that LipiORDER and Laurdan respond differently to the same temperature change. The ratio of LipiORDER was obtained from a single GUV during the thermal deformation and was taken in step with the morphological values, whereas the GP_{340} value represents the mean values of GUVs under a pseudo-equilibrium state. Another reason may be the difference in the location of the respective fluorescent probes in the membrane; the fluorophore of Laurdan is located under the acyl chain of the phospholipid in the membrane. The exact location of LipiORDER remains unknown; however, simulations have shown that its parent molecule, pyrene, is widely distributed around the hydrophobic portion of the membrane.[45] At the end of the morphological change, the formation of daughter vesicles were observed. After daughter formation, the parent vesicle continued to increase in size, and the fluorescence intensity ratio of LipiORDER in the parent vesicle increased slightly, as shown in Fig. 5-iii and iv.

Above the transition temperature (T_m), the LipiORDER ratio reached a peak and maintained a constant value. The same trend was observed for the morphological parameters, normalized area, and diameter, which reached a peak value at approximately the same time. The small fluctuations in area and diameter were due to either rotation or small movements of the vesicle caused by the high fluidity at this point. Until the cooling phase started at 180 s, the values of the LipiORDER ratio and structural parameters were conserved. However, the expected GP_{340} value underwent a large change at this temperature difference (Fig. 5-v and vi). Furthermore, the increase of the hydration degree (the decreasing of GP_{340}) did not change the morphological values.

After the cooling phase was initiated at 180 s, the physical parameters and fluorescence ratio values of LipiORDER responded similarly to the temperature change again and showed a steep decrease in all three values. As stated earlier, this cooling phase caused a rapid decrease in the area per lipid and thus led to an increase in membrane tension, finally resulting in the formation of pores. After the formation of the pore, there was still a small decrease in size and the fluorescence ratio values of LipiORDER of the parent vesicle until the passing of the T_m on the cooling phase. Upon passing T_m, the physical parameters and fluorescence ratio values of LipiORDER followed a similar trend. The fluorescence ratio values of LipiORDER and vesicle size did not change until the end of the temperature cycle, despite the change in temperature above 10 °C. Interestingly, GUVs exhibited different responses, such as different ratio variation rates and structural variation during the temperature cycle in heating to T_m from 20 °C or cooling to 20 °C from T_m. The birth of the daughter vesicle and changing state of the membrane during the temperature cycle may have caused this difference but the lipid membrane may also respond differently to passing over the T_m from heating than it does from cooling.

In addition, single GUV analysis using our method allowed inference of the parent vesicle composition before and after the thermal cycle. The fluorescence ratio values of the (80/20) parent vesicles before and after the thermal cycle were 0.44 and 0.42, respectively, as shown in Fig. 4. From the fluorescence ratio values in both the daughter and parent vesicles, it can be inferred that the composition of the parent vesicles after the thermal cycle was less DPPC and between 80/20–70/30 (DPPC/OA). This is also consistent with the fact that the increase in OA had no significant variation in the ratio values.

During deformation, there may be a variety of other factors that affect the progression of the phenomena, such as the pK_a of OA and its variability over the tested temperature range. The pK_a of various fatty acids embedded in bilayers was calculated *via* simulation to be approximately 7, indicating that there is approximately half OA in its anionic form and half in its neutral form.[46,47] The protonation of OA affects its molecular shape by changing it from an inverse cone shape to a cylindrical shape. This is caused by pH changes and induces large deformations

in fatty acid membranes.[6] However, in this study, the pH was not significantly changed under temperature variation;[48] thus, the effect of the OA shape variation can be neglected.

The rate of temperature change may also affect deformation. By reducing the cooling rate, the rate of morphological shrinkage of the membrane also decreases. This will cause the increase of membrane tension to slow, which may inhibit the formation of the pore. Studies under a slower rate of temperature change showed a completely different type of deformation and domain formation in DPPC GUVs.[37] In our case, a similar pattern was observed in approximately 5% of all deformation trials, as shown in the ESI,† Movie S5. A physical interpretation of this phenomenon is outside the scope of this study; however, it most likely arises from the slow increase in membrane tension, which is balanced by the line tension generated by domain formation.[49] As the rate of heating is slowed, there will come a point where the rate of heating is sufficiently slow enough that the vesicle will reach a pseudo-equilibrium at each temperature and no deformation will be observed.

3.5 Membrane properties greatly influence daughter formation

Through the analysis of membrane properties such as hydrophobicity and membrane packing with fluorescent probes and the simple structural parameters, some insights about the bilayer membrane can be explicated. Fig. 6 shows the confocal images of a vesicle undergoing a temperature cycle. In addition, the full time-lapse of these images is shown in the ESI,† Movies S6 and S7. Before heating, the vesicles were in a stable gel phase[50] and exhibited minimal fluctuations and movement of the membrane during this period, as shown in Fig. 6(i). Upon heating, vesicles undergo membrane remodeling, leading to the lateral movement of OA to certain areas, and this lateral movement can be exemplified by the lateral movement of the lipid species within a single leaflet. This is similar to the formation of domains in other multicomponent GUV systems, where manipulation of the temperature changes the packing and ordering of the lipid membrane and causes domain formation and restructuring,[51] as shown in Fig. 6(ii). In addition, MD simulations have revealed that the flip-flop of lipid species is one of the most important factors determining the deformation of lipid membranes.[3] However, fatty acids have an incredibly fast flip-flop rate (on the order of microseconds) compared to normal phospholipids (on the order of hours).[52] Due to this fast flip-flop rate, OA can be assumed to be in an equivalent concentration in the inner and outer leaflets; thus, the asymmetric distribution of OA in the inner and outer leaflets of the membrane is not a contributing factor to the deformation of the membrane.

This lateral movement phenomenon resulted in OA grouping into specific areas of the GUV. This can be interpreted from the previous LipiORDER ratio data presented in Fig. 4, which shows that the daughter vesicles have a much lower percentage of OA than the parents they are born from. The OA in the region where daughter vesicles most likely exhibited some lateral movement within the membrane to other regions before the budding phenomena occurs to form small nanodomains of highly concentrated OA. The presence of nanodomains in the binary mixture has been shown in wet research and MD simulations reported nanodomain formation in DPPC/OA mixtures as well.[53,54] During this period of high temperature the membrane is mainly in the liquid disordered phase and has a sufficiently high diffusion coefficient, therefore the presence of the lateral diffusion of lipid molecules is to be expected. The increasing local concentration of OA in these other regions induces a much higher curvature than that observed in wholly DPPC regions.[39] These membrane regions with highly concentrated OA induced a large change in curvature due to the inverse cone shape of OA within the membrane inducing a greater curvature than the naturally flat membrane of purely DPPC, as shown in Fig. 6-iii. For clarity, the image presented here displays only the formation of a large daughter vesicle. However, in most cases, multiple regions of high curvature formed daughter vesicles causing the creation of multiple daughter vesicles. This melds well with the highly-documented phenomena of the dynamic behavior of the lipid membrane especially while passing over the phase transition of the lipid membrane inducing various changes, including the formation of domains.[55]

These high curvature regions and the formation of a daughter vesicle cause increased stress on the rest of the membrane due to the irregular shape. In an attempt to help restore the vesicle to the lower energy state of a sphere the two high-curvature regions of the preformed daughter vesicles gradually grow closer and finally close. Thus, the formation singular bilayer string that connects the parent and fully formed daughter vesicle occurs and this can be visualized, as shown in the cartoon (Fig. 6-iv). Long string-like bilayers of high-curvature lipids, such as OA, have been previously reported to be unstable and easily break when connecting the parent and daughter vesicles.[56] The release of this OA string most likely causes the OA to reintegrate into the parent vesicle. After the formation of the daughter vesicle, the membrane grew in size slightly as seen in Fig. 5-v until the transition temperature.

Upon further examination of the data presented in Fig. 5, it is apparent that there may be a direct relationship between the membrane's interfacial properties and the physical parameters presented. Therefore, a detailed analysis was conducted in three periods (i–ii, iii–v, and vi–vii) regarding the relationship between the morphology (deformation) and membrane hydrophobicity. Fig. 6(A)–(C) show the plots comparing the measured area of the vesicles *versus* the ratio values of LipiORDER during the displayed period of the deformation cycle. The R^2 values of these relationships range from 0.62–0.95, thus these values do not prove any strong relationship between the membrane hydrophobicity and morphology in the three periods (i–ii, iii–v, vi–vii). Nonetheless, further probing the connection between the interfacial membrane properties and physical parameters of the membrane may prove beneficial. Fig. 5 presents two variations of membrane measurements, expected GP_{340} and LipiORDER, however, only comparative analysis between LipiORDER and normalized area was undertaken. This is due to the expected GP_{340} value not being measured in step

with the deformation and being an extrapolation of the GP_{340} value based on temperature. Nonetheless, a comparison between the expected GP_{340} value and normalized area is presented in the ESI,† in Fig. S5 accompanied by a complementary analysis.

Taking a look at Fig. 6(A) corresponding to the interval between i and ii with the activity of the membrane's behavior during this region of the deformation cycle in mind, it can be observed that LipiORDER responds in a strong relationship with the quick increase of fluidity of the membrane during this time period. The membrane undergoes many fluctuations in its shape, leading to a noncircular shape owing to the influx of water and the lateral movement of OA, causing the overall packing of the membrane to rapidly increase. Moving on to the next period of note, iii to iv, or the period where the daughter vesicle is formed and the membrane expands and reaches its highest temperature, as shown in Fig. 6(B), the relationship between the ratio of LipiORDER and normalized area during this period was the weakest in the entire deformation cycle. During this period, the membrane rapidly increased in size, with an increase of over 30%, whereas the ratio of LipiORDER slightly increased. This region of the deformation is also marked by slight fluctuations in the normalized area and ratio value due to rotation of the vesicle in solution and standard error of the ratio measurement system, respectively, leading to the mildly weak relationship found in Fig. 6(B). The final period, the interval of vi–vii, reveals the strongest relationship found in Fig. 6(C); during this period, the membrane undergoes rapid shrinking owing to the cooling temperature and transitions back into the solid ordered phase. The fluorescence ratio of LipiORDER and normalized area were almost perfectly in step during this time period. This is because of the steady shrinking of the membrane area, which directly corresponds to lowering the fluidity of the membrane.

There is a negative slope during the i-ii region and a positive slope with the remaining two regions, iii–v and vi, vii. The first region, Fig. 6(A), exemplified by the sole holder of a negative slope is due to the mild deformation in the form of pinching of the membrane leading to a smaller normalized area, and later the interior budding phenomena. Furthermore, a rapid increase in the LipiORDER value, signifying a more loosely packed membrane, leads to a negative slope. The second region, Fig. 6(B), can almost be characterized as a flat slope and this is due to the changes in this region specifically due to fluctuations within the membrane at the higher temperature, particularly the normalized area as the GUV is rotating and moving within the solution. The final region, Fig. 6(C), is strongly positively correlated, and the fast change in the lipid packing measured by LipiORDER and the rapid shrinking in the membrane size lead to this steep positive slope.

4. Conclusion

The deformation and subsequent birthing of the vesicles were studied based on membrane hydrophobicity, packing and morphological parameters in a time-lapse manner under thermally induced deformation. Fluorescence ratiometric analysis with simultaneous dual-wavelength detection showed different behaviors in GUVs with different membrane packing under thermal cycling and enabled inferences of the daughter vesicle composition and the membrane's local composition during deformation. The significant results of this novel analysis technique demonstrated the relationship in membrane morphology and membrane packing during thermally induced deformation and showed that the ratio of OA in the daughter vesicles was lower than that in the parents *via* the interpretation of the pre and post deformation Lipi-ORDER. In addition, OA lateral movement is the primary contributor to daughter vesicle formation. Thus, the combination of our methodology (*in situ* quantitative membrane property–morphology relation (QmPMR) analysis) and traditional mechanical analysis will be used to further understand cell membrane deformation and allow researchers to gain deeper insights into cellular processes, such as endocytosis and exocytosis.

Author contributions

Y. O. and Z. N. planned the study and designed the experiments. Z. N. performed the experiments, and all authors analyzed the data. Y. O. and Z. N. wrote the manuscript, and all authors reviewed it. All authors (Z. N., Y. O., N. M. W., G. L. T., and H. U.) have read and agreed with this version.

Conflicts of interest

The authors declare no competing financial interests.

Acknowledgements

This work was supported by JSPS KAKENHI (JP21H04628, 18H02005) and the Grant-in-Aid for Transformative Research Areas (A) ''Material Symbiosis'' (20H05874) from MEXT, Japan. One of the authors (Y. O.) thanks JKA and its promotion funds from KEIRIN RACE, Multidisciplinary Research Laboratory System in Osaka University, Tateisi Science and Technology Foundation, Mukai Science and Technology Foundation, and Toyota Physical and Chemical Research Institute. One author (Z. N.) thanks the Japanese Government for the MEXT scholarship.

References

1 D. L. Bader and M. M. Knight, Biomechanical analysis of structural deformation in living cells, *Med. Biol. Eng. Comput.*, 2008, **46**(10), 951–963.
2 T. Harayama and H. Riezman, Understanding the diversity of membrane lipid composition, *Nat. Rev. Mol. Cell Biol.*, 2018, **19**(5), 281–296.
3 N. Urakami, Y. Sakuma, T. Chiba and M. Imai, Vesicle deformation and division induced by flip-flops of lipid molecules, *Soft Matter*, 2021, **17**(37), 8434–8445.

4 M. Imai, Y. Sakuma, M. Kurisu and P. Walde, From vesicles toward protocells and minimal cells, *Soft Matter*, 2022, **18**(26), 4823–4849.
5 Y. Sakuma and M. Imai, Model System of Self-Reproducing Vesicles, *Phys. Rev. Lett.*, 2011, **107**(19), 5.
6 K. Ikari, Y. Sakuma, T. Jimbo, A. Kodama, M. Imai and P. A. Monnard, *et al.*, Dynamics of fatty acid vesicles in response to pH stimuli, *Soft Matter*, 2015, **11**(31), 6327–6334.
7 K. Kurihara, M. Tamura, K. Shohda, T. Toyota, K. Suzuki and T. Sugawara, Self-reproduction of supramolecular giant vesicles combined with the amplification of encapsulated DNA, *Nat. Chem.*, 2011, **3**(10), 775–781.
8 S. Emami, W. C. Su, S. Purushothaman, V. N. Ngassam and A. N. Parikh, Permeability and Line-Tension-Dependent Response of Polyunsaturated Membranes to Osmotic Stresses, *Biophys. J.*, 2018, **115**(10), 1942–1955.
9 Y. Dreher, K. Jahnke, E. Bobkova, J. P. Spatz and K. Gopfrich, Division and Regrowth of Phase-Separated Giant Unilamellar Vesicles, *Angew. Chem., Int. Ed.*, 2021, **60**(19), 10661–10669.
10 I. Gozen, E. S. Koksal, I. Poldsalu, L. Xue, K. Spustova and E. Pedrueza-Villalmanzo, *et al.*, Protocells: Milestones and Recent Advances, *Small*, 2022, **18**(18), 32.
11 J. Bigay and B. Antonny, Curvature, Lipid Packing, and Electrostatics of Membrane Organelles: Defining Cellular Territories in Determining Specificity, *Dev. Cell*, 2012, **23**(5), 886–895.
12 P. Khunpetch, Y. Sakuma, M. Imai and T. Kawakatsu, Birthing of a daughter vesicle in a model system for self-reproduction vesicles, *Phys. Fluids*, 2021, **33**, 077103.
13 N. Watanabe, Y. Goto, K. Suga, T. K. M. Nyholm, J. P. Slotte and H. Umakoshi, Solvatochromic Modeling of Laurdan for Multiple Polarity Analysis of Dihydrosphingomyelin Bilayer, *Biophys. J.*, 2019, **116**(5), 874–883.
14 N. Watanabe, K. Suga and H. Umakoshi, Functional Hydration Behavior: Interrelation between Hydration and Molecular Properties at Lipid Membrane Interfaces, *J. Chem.*, 2019, **2019**, 15.
15 I. K. Jarsch, F. Daste and J. L. Gallop, Membrane curvature in cell biology: An integration of molecular mechanisms, *J. Cell Biol.*, 2016, **214**(4), 375–387.
16 S. Mukerjee, A. S. Saeedan, M. N. Ansari and M. Singh, Polyunsaturated Fatty Acids Mediated Regulation of Membrane Biochemistry and Tumor Cell Membrane Integrity, *Membranes*, 2021, **11**(7), 15.
17 A. Gupta, M. Kallianpur, D. S. Roy, O. Engberg, H. Chakrabarty and D. Huster, *et al.*, Different membrane order measurement techniques are not mutually consistent, *Biophys. J.*, 2023, **122**(6), 964–972.
18 E. G. Kelley, P. D. Butler, R. Ashkar, R. Bradbury and M. Nagao, Scaling relationships for the elastic moduli and viscosity of mixed lipid membranes, *Proc. Natl. Acad. Sci. U. S. A.*, 2020, **117**(38), 23365–23373.
19 S. S. W. Leung, J. Brewer, L. A. Bagatolli and J. L. Thewalt, Measuring molecular order for lipid membrane phase studies: Linear relationship between Laurdan generalized polarization and deuterium NMR order parameter, *Biochim. Biophys. Acta, Biomembr.*, 2019, **1861**(12), 183053.
20 G. van Meer, D. R. Voelker and G. W. Feigenson, Membrane lipids: where they are and how they behave, *Nat. Rev. Mol. Cell Biol.*, 2008, **9**(2), 112–124.
21 Y. Sakuma, T. Taniguchi, T. Kawakatsu and M. Imai, Tubular Membrane Formation of Binary Giant Unilamellar Vesicles Composed of Cylinder and Inverse-Cone-Shaped Lipids, *Biophys. J.*, 2013, **105**(9), 2074–2081.
22 T. Jimbo, Y. Sakuma, N. Urakami, P. Ziherl and M. Imai, Role of Inverse-Cone-Shape Lipids in Temperature-Controlled Self-Reproduction of Binary Vesicles, *Biophys. J.*, 2016, **110**(7), 1551–1562.
23 K. Morigaki, S. Dallavalle, P. Walde, S. Colonna and P. L. Luisi, Autopoietic self-reproduction of chiral fatty acid vesicles, *J. Am. Chem. Soc.*, 1997, **119**(2), 292–301.
24 S. Aryal, S. Hussain, C. A. Drevon, E. Nagelhus, O. Hvalby and V. Jensen, *et al.*, Omega-3 fatty acids regulate plasticity in distinct hippocampal glutamatergic synapses, *Eur. J. Neurosci.*, 2019, **49**(1), 40–50.
25 Y. Okamoto, K. Hamaguchi, M. Watanabe, N. Watanabe and H. Umakoshi, Characterization of Phase Separated Planar Lipid Bilayer Membrane by Fluorescence Ratio Imaging and Scanning Probe Microscope, *Membranes*, 2022, **12**(8), 770.
26 Z. Boban, I. Mardesic, W. K. Subczynski and M. Raguz, Giant Unilamellar Vesicle Electroformation: What to Use, What to Avoid, and How to Quantify the Results, *Membranes*, 2021, **11**(11), 17.
27 T. J. Politano, V. E. Froude, B. X. Jing and Y. X. Zhu, AC-electric field dependent electroformation of giant lipid vesicles, *Colloids Surf., B*, 2010, **79**(1), 75–82.
28 V. Betaneli, R. Worch and P. Schwille, Effect of temperature on the formation of liquid phase-separating giant unilamellar vesicles (GUV), *Chem. Phys. Lipids*, 2012, **165**(6), 630–637.
29 J. Valanciunaite, E. Kempf, H. Seki, D. I. Danylchuk, N. Peyrieras and Y. Niko, *et al.*, Polarity Mapping of Cells and Embryos by Improved Fluorescent Solvatochromic Pyrene Probe, *Anal. Chem.*, 2020, **92**(9), 6512–6520.
30 Y. Okamoto, Y. Kishi, K. Suga and H. Umakoshi, Induction of Chiral Recognition with Lipid Nanodomains Produced by Polymerization, *Biomacromolecules*, 2017, **18**(4), 1180–1188.
31 N. F. Morales-Penningston, J. Wu, E. R. Farkas, S. L. Goh, T. M. Konyakhina and J. Y. Zheng, *et al.*, GUV preparation and imaging: Minimizing artifacts, *Biochim. Biophys. Acta, Biomembr.*, 2010, **1798**(7), 1324–1332.
32 G. Gunther, L. Malacrida, D. M. Jameson, E. Gratton and S. A. Sanchez, LAURDAN since Weber: The Quest for Visualizing Membrane Heterogeneity, *Acc. Chem. Res.*, 2021, **54**(4), 976–987.
33 T. Inoue, S. Yanagihara, Y. Misono and M. Suzuki, Effect of fatty acids on phase behavior of hydrated dipalmitoylphosphatidylcholine bilayer: saturated versus unsaturated fatty acids, *Chem. Phys. Lipids*, 2001, **109**(2), 117–133.
34 J. Steinkuhler, E. Sezgin, I. Urbancic, C. Eggeling and R. Dimova, Mechanical properties of plasma membrane vesicles correlate with lipid order, viscosity and cell density, *Commun. Biol.*, 2019, **2**, 8.

35 S. A. Akimov, P. E. Volynsky, T. R. Galimzyanov, P. I. Kuzmin, K. V. Pavlov and O. V. Batishchev, Pore formation in lipid membrane II: Energy landscape under external stress, *Sci. Rep.*, 2017, **7**, 20.

36 J. Kas and E. Sackmann, Shape Transitions And Shape Stability Of Giant Phospholipid-Vesicles In Pure Water Induced By Area-To-Volume Changes, *Biophys. J.*, 1991, **60**(4), 825–844.

37 R. L. Knorr, J. Steinkuhler and R. Dimova, Micron-sized domains in quasi single-component giant vesicles, *Biochim. Biophys. Acta, Biomembr.*, 2018, **1860**(10), 1957–1964.

38 D. Koller and K. Lohner, The role of spontaneous lipid curvature in the interaction of interfacially active peptides with membranes, *Biochim. Biophys. Acta, Biomembr.*, 2014, **1838**(9), 2250–2259.

39 A. I. I. Tyler, J. L. Greenfield, J. M. Seddon, N. J. Brooks and S. Purushothaman, Coupling Phase Behavior of Fatty Acid Containing Membranes to Membrane Bio-Mechanics, *Front. Cell Dev. Biol.*, 2019, **7**, 10.

40 E. Karatekin, O. Sandre, H. Guitouni, N. Borghi, P. H. Puech and F. Brochard-Wyart, Cascades of transient pores in giant vesicles: Line tension and transport, *Biophys. J.*, 2003, **84**(3), 1734–1749.

41 J. Brewer, J. B. de la Serna, K. Wagner and L. A. Bagatolli, Multiphoton excitation fluorescence microscopy in planar membrane systems, *Biochim. Biophys. Acta, Biomembr.*, 2010, **1798**(7), 1301–1308.

42 M. L. Jacobs, H. A. Faizi, J. A. Peruzzi, P. M. Vlahovska and N. P. Kamat, EPA and DHA differentially modulate membrane elasticity in the presence of cholesterol, *Biophys. J.*, 2021, **120**(11), 2317–2329.

43 D. I. Danylchuk, E. Sezgin, P. Chabert and A. S. Klymchenko, Redesigning Solvatochromic Probe Laurdan for Imaging Lipid Order Selectively in Cell Plasma Membranes, *Anal. Chem.*, 2020, **92**(21), 14798–14805.

44 Y. Miele, G. Hollo, I. Lagzi and F. Rossi, Shape Deformation, Budding and Division of Giant Vesicles and Artificial Cells: A Review, *Life*, 2022, **12**(6), 20.

45 H. A. L. Filipe, M. J. Moreno and L. M. S. Loura, The Secret Lives of Fluorescent Membrane Probes as Revealed by Molecular Dynamics Simulations, *Molecules*, 2020, **25**(15), 3424.

46 S. Skulj and M. Vazdar, Calculation of apparent p*K*(a) values of saturated fatty acids with different lengths in DOPC phospholipid bilayers, *Phys. Chem. Chem. Phys.*, 2019, **21**(19), 10052–10060.

47 R. M. Thomas, A. Baici, M. Werder, G. Schulthess and H. Hauser, Kinetics and mechanism of long-chain fatty acid transport into phosphatidylcholine vesicles from various donor systems, *Biochemistry*, 2002, **41**(5), 1591–1601.

48 J. Kurniawan, K. Suga and T. L. Kuhl, Interaction forces and membrane charge tunability: Oleic acid containing membranes in different pH conditions, *Biochim. Biophys. Acta, Biomembr.*, 2017, **1859**(2), 211–217.

49 N. Wongsirojkul, A. Masuta, N. Shimokawa and M. Takagi, Control of Line Tension at Phase-Separated Lipid Domain Boundaries: Monounsaturated Fatty Acids with Different Chain Lengths and Osmotic Pressure, *Membranes*, 2022, **12**(8), 12.

50 N. Shimokawa, R. Mukai, M. Nagata and M. Takagi, Formation of modulated phases and domain rigidification in fatty acid-containing lipid membranes, *Phys. Chem. Chem. Phys.*, 2017, **19**(20), 13252–13263.

51 U. Bhojoo, M. Chen and S. Zou, Temperature induced lipid membrane restructuring and changes in nanomechanics, *Biochim. Biophys. Acta, Biomembr.*, 2018, **1860**(3), 700–709.

52 C. Y. Wei and A. Pohorille, Flip-Flop of Oleic Acid in a Phospholipid Membrane: Rate and Mechanism, *J. Phys. Chem. B*, 2014, **118**(45), 12919–12926.

53 K. Suga and H. Umakoshi, Detection of Nanosized Ordered Domains in DOPC/DPPC and DOPC/Ch Binary Lipid Mixture Systems of Large Unilamellar Vesicles Using a TEMPO Quenching Method, *Langmuir*, 2013, **29**(15), 4830–4838.

54 J. Cerezo, J. Zuniga, A. Bastida, A. Requena and J. P. Ceron-Carrasco, Atomistic Molecular Dynamics Simulations of the Interactions of Oleic and 2-Hydroxyoleic Acids with Phosphatidylcholine Bilayers, *J. Phys. Chem. B*, 2011, **115**(40), 11727–11738.

55 T. Heimburg, The excitable fluid mosaic, *Biochim. Biophys. Acta, Biomembr.*, 2023, **1865**(3), 11.

56 C. S. Poojari, K. C. Scherer and J. S. Hub, Free energies of membrane stalk formation from a lipidomics perspective, *Nat. Commun.*, 2021, **12**(1), 10.